RSC Advances

PAPER

View Article Online
View Journal | View Issue

Cite this: *RSC Adv.*, 2015, **5**, 15172

Microfluidic spinning of fibrous alginate carrier having highly enhanced drug loading capability and delayed release profile

S. Y. Ahn,†[a] C. H. Mun†[a] and S. H. Lee*[ab]

Natural polymer-based drug carriers have been developed for antimicrobial applications but several problems remain with their poor controllability of drug loading and degradation. We introduce a novel method to produce improved antibiotic alginate fiber with high drug entrapment properties and a delayed degradation profile. A microfluidic spinning system with a low-polarity isopropyl alcohol (IPA) sheath flow was used to dehydrate an alginate/ampicillin aqueous solution and to form densely packed fiber with enhanced drug loading efficiency. The amounts of ampicillin initially loaded in the IPA-fiber were much higher than in the conventional water-based fiber and they released a more prolonged profile. The fibers were characterized by analyzing the morphology, mass loss and structural properties. The fibers were also used for an *in vivo* infected wound healing study. The results showed that the IPA-based fibrous alginate drug carrier possesses superior properties for loading drugs and potentials for wound healing applications with easy management.

Received 29th September 2014
Accepted 19th December 2014

DOI: 10.1039/c4ra11438h

www.rsc.org/advances

Introduction

The targeted delivery of a drug to a specific region and its controlled release over long periods have been critical aims in the pharmaceutical industry toward enhancing patients' compliance and the therapeutic efficacy of pharmaceutical agents. In recent decades, a variety of biodegradable controlled release drug carrier technologies have been developed using simple and cost-effective processes.[1,2] Despite a splendid progress in these technologies, the loading of drugs as large as possible and release of drugs for long duration still remains a critical issue. Diverse biodegradable drug carriers for use in living organisms have been developed based on several promising natural and synthetic polymers, lipids, surfactants, and dendrimers.[3–5] Natural polysaccharides, such as chitosan, alginate, and starch, have been broadly used in the pharmaceutical and biomedical industries as drug carriers and scaffolds. These natural biomaterials can incorporate drugs and be delivered by oral administration or implantation, with the subsequent gradual degradation and diffusion of the drugs into the living organism.[6–8]

Among these materials, alginate has been extensively employed as a biopolymer drug carrier material due to its low toxicity, biodegradability, high biocompatibility to the host, and the safe gelation with divalent cations under mild conditions.[9,10] Furthermore, the ability of alginate to form various conditioned gels enabled the large-scale and well-organized fabrication of drug-embedded carriers through simple and cost-effective processes, with the subsequent controlled release of the embodied drug. Despite these huge advantages, alginate faces several hurdles before it may be widely used as a drug carrier. Recent progress in microfabrication technologies allows the mass production of micro- or nano-scale microstructures (*e.g.*: particle, fiber and tube), which may overcome several limits of alginate drug carrier. However, there still remain some problems to be resolved. First, the handling of size-controlled microstructures and the construction of macroscale shapes (*e.g.*: patch shape) by assembling microstructures are difficult. Second, the swelling and the degradation at a certain ratio of alginate could cause fast diffusion of the loaded drugs, which in turn, can result in burst releases in aqueous media or the body.[11,12] In particular, the alginate microparticles degrade rapidly, and that makes it unsuitable for commercial use despite its excellent features as drug carrier; therefore, delaying the degradation profiles remains a significant challenge. Third, an effective carrier requires uniform loading of the drug in as sufficient quantities as possible. However, the alginate in aqueous condition does not satisfy these requirements because it is easily swollen, and thus cannot carry the sufficient amount of drug. Nowadays, some of these problems have been addressed and improved by blending the alginate with other materials,[13–16] but not all of these complications have yet been resolved.

[a]*Department of Biomedical Engineering, College of Health Science, Korea University, Jeongeug-dong, Seongbuk-gu, Seoul, 136-703, Republic of Korea. E-mail: dbiomed@korea.ac.kr*

[b]*KU-KIST Graduate School of Converging of Sciences & Technologies, Korea University, Seoul 136-713, Republic of Korea*

† These authors contributed equally.

This paper describes a microfluidically-spun fibrous alginate carrier, the degradation of which can be delayed in a controllable manner and the drug-loading capability of which is highly enhanced. Recent progress in microfluidic technology has allowed the mass production of micro- and nano-scale fibrous and tubular structures without the use of complicated devices or facilities.[17–19] The microfluidic spinning systems enabled the physicochemical coding with various composition and morphology on continuous fibers, and are emerging as advanced tools for a variety of applications in tissue engineering, drug delivery and cell biology.[20–23] Here, we have demonstrated the production of fibers with highly enhanced drug loading capability by using a microfluidic platform and by changing sheath flow with different polarity. The performance of the material as a drug carrier was demonstrated by loading ampicillin, a representative model drug, to the alginate fibers. The loading capability of the drug was enhanced by high and compact ordering of the polymer chain using isopropyl alcohol (IPA) as a sheath flow. Unlike the water-based sheath flow, the IPA-based sheath flow facilitated the highly condensed aggregation of alginate polymer chains,[24,25] which minimized the swelling, while entrapping the drug within the fibrous matrix as large as possible. The highly ordered fiber structure contributed to the delayed degradation. To slow down the degradation process more, drug-loaded fibers were immersed in a calcium ion bath to increase the degree of cross-linking within the alginate network. A previous study reported that adequately calcium cross-linked fibers were mechanically stronger and displayed prolonged degradation times compared to the less cross-linked fibers.[26–28] The curing time for the alginate fibers mediates the calcium ion cross-linking of the polymer chains, and thus governs the degree of crosslinking.[29] The efficacy of the fibers as a drug carrier was determined by measuring the morphological profile of the fibers during the drug release, and the effectiveness of the ampicillin-loaded fibers was tested by placing them on a bacteria growing dish. For *in vivo* evaluation, a chitosan patch containing ampicillin-laden fibers was placed on a wounded site of a mouse infected with bacteria, and the wound-healing effect by the drug-laden patch was observed. The proposed microfluidic spinning method enables the high loading capability of drugs and will be broadly applied for the efficient delivery of diverse drugs.

Materials and methods

Materials

A 3% (w/w) sodium alginate solution was prepared by dissolving alginic acid powder (Sigma, St. Louis, MO, USA) in deionized water (DW). 100 mg of ampicillin sodium salt (Sigma, St. Louis, MO, USA) was mixed with 1 mL alginate solution as the core flow. Sheath solution containing 3% (w/w) $CaCl_2$ in DW and IPA (Sigma, St. Louis, MO, USA) was prepared to induce the instant gelation of alginate solutions. Solutions containing 10% (w/w) $CaCl_2$ in DW and IPA were used for curing of fibers in coagulation baths to enhance crosslinking. The solutions were purified by filtration (Dismic 25CS020AS, Advantec Toyo Co., Tokyo, Japan). Microfluidic chips were fabricated using an SU-8 patterned photoresist mold. The PDMS pre-polymer and the crosslinker (Sylgard 184, Dow Corning) were mixed in a 10 : 1 ratio, poured onto the mold, and cured at 75 °C for at least 20 min. The PDMS substrates were then bonded together using the oxygen plasma treatment. A *staphylococcus aureus* (*S. aureus*) strain ATCC®25923 was purchased from American Type Culture Collection (Manassas, VA, USA). Tryptic soy broth and agar were purchased from BD Diagnostic Systems.

Preparation of antibiotic fibers

The fibers containing ampicillin were fabricated in a PDMS microfluidics chip bearing cylindrical and coaxial flow channels.[30] Four distinct fiber-spinning conditions were applied: two different sheath fluids were used either in the presence or absence of the treatment in a calcium coagulation bath. Continuous microfibers were produced through the PDMS microchip using a core fluid containing 2 g of ampicillin sodium salt in 20 mL of 3% w/v alginate solution and one of two sheath fluids—(3% $CaCl_2$-DW (Fig. 1a) or 3% $CaCl_2$-IPA (Fig. 1b)). The two types of drug-loaded fibers spun with two different sheath solutions were collected and stored under two different conditions, thus preparing four types of sample fibers in total. The first fiber sample was fabricated using 3% $CaCl_2$-IPA sheath solution and immediately washed with pure IPA without curing process to enhance crosslinking (named as IPA-0 h-fiber). The second sample fiber was spun using 3% $CaCl_2$-IPA sheath solution and cured in 10% $CaCl_2$-IPA bath for further crosslinking with calcium ions. After 24 hours, this second fiber sample was washed in pure IPA (named as IPA-24 h-fiber). The third sample fiber was fabricated using 3% $CaCl_2$-DW sheath solutions and was immediately washed with deionized water (named as DW-0 h-fiber). The fourth sample fiber was spun using 3% $CaCl_2$-DW sheath solution and cured in a 10% $CaCl_2$-DW bath for 24 hours and washed with deionized water (named as DW-24 h-fiber). For storage, the DW-based groups (DW-0 h-fiber and DW-24 h-fiber) were dehydrated using a series of graded ethanol (50, 70, 95, and 100%) solutions and were dried at ambient conditions. The IPA-based groups (IPA-0 h-fiber and IPA-24 h-fiber) were dried at room temperature after formation because they had already been dehydrated. The fibers were imaged using green fluorescent polystyrene microspheres (300 nm size PS bead, Thermo, Fremont CA, USA) in place of the ampicillin sodium salt to demonstrate the loading capability.

Morphological characterization

The morphologies of the fibers were observed using scanning electron microscopy (SEM). The changes in the four groups (DW-0 h-fiber, DW-24 h-fiber, IPA-0 h-fiber and IPA-24 h-fiber) of drug-loaded fibers were examined after they had been immersed in phosphate buffered saline (PBS), which has an ionic condition similar to that of the human body. Each sample fibers were stored for 7 days to give them sufficient time for hydration and ionic interaction between alginate matrix and media. The hydrated fibers were processed for imaging on the 7^{th} day by washing and dehydrating the fibers in a series of graded ethanol solutions (50, 70, 95, and 100%) and dried at RT

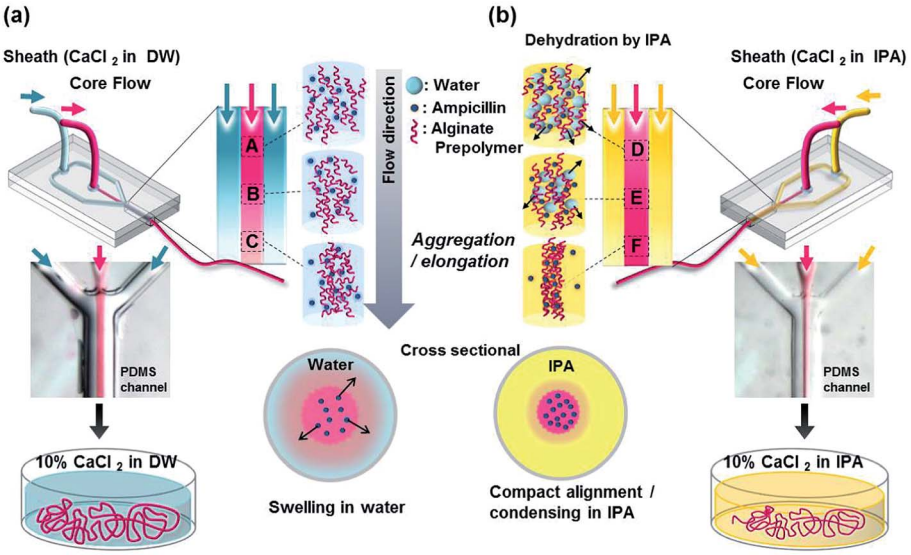

Fig. 1 Schematic diagram showing the loading of drugs into the alginate fibers. The polymers aggregated and encapsulated the drug molecules along the flow direction of each channel. (a) Fiber formation using the water sheath fluid, and further fiber coagulation in a calcium ion solution. (b) Fiber formation *via* dehydration by the IPA sheath fluid, and further fiber coagulation in a calcium ion solution.

for 1 day. The fiber samples were fixed on conductive carbon tape and sputter-coated with a thin gold/palladium (Au/Pd) layer. The prepared samples were observed using SEM (JSM-5600LV SEM, Tokyo, Japan) at an acceleration of 10 kV.

Degradation determination

The extent of degradation was characterized by immersing a certain quantity of each sample fibers in PBS at 37 °C. After a fixed time interval, the fibers were washed and dried in an oven at 75–80 °C, allowed to cool under ambient conditions, and their weight was measured. The drying step was continued until a constant weight was achieved. The degree of fiber degradation was represented by the mass loss, calculated with the following equation:

$$\text{Mass loss } (\%) = [(W_i - W_f)/W_i] \times 100\%,$$

where W_i denotes the initial starting weight of the fiber, and W_f is the weight of the partially eroded sample. All experiments were performed in triplicate.

In vitro ampicillin release studies

The *in vitro* release of ampicillin from the fibers was investigated by measuring the concentration of ampicillin released into the PBS solution at RT. The alginate fibers loaded with ampicillin were immersed in a 12 well plate containing 5 mL PBS for 7 days. At each predetermined time interval, a given volume of solution was withdrawn, and the amount of ampicillin released from the drug-loaded fibers was measured using the UV absorbance spectrophotometry (Optizen POP; Mecasys, Daejeon, Korea) at 200 nm. The volume of the solution removed was replaced with fresh PBS to maintain a constant total volume.

Fourier transform infrared spectroscopy (FT-IR) analysis

To characterize the surface properties of pure alginate powder, DW-24 h-fiber and IPA-24 h-fiber, FT-IR spectroscopy was performed, equipped with a Universal ATR diamond accessory of Perkin Elmer Spectrum 100 (Perkin Elmer, MA, USA). Transmission and ATR spectra were recorded with 10 scans at a resolution of 4 cm^{-1} between 4000 and 800 cm^{-1}.

XRD analysis

In order to investigate the crystallinity of DW-24 h-fiber and IPA-24 h-fiber, XRD analysis was done using a D/max-2500 X-ray diffractometer (Rigaku, Tokyo, Japan) equipped with a Cu kα source. The one-dimensional X-ray diffraction patterns with the intensity curves, and a function of 2θ, the scattering angle, were obtained from integrating the two-dimensional scattering patterns of each sample.

Antibiotic activity test

Antibiotic activity tests were conducted based on the modified Kirby–Bauer Disc method.[31] For the test, two types of drug loaded fiber were prepared: DW-24 h-fiber and IPA-24 h-fiber fabricated using the sample solution of 1 mg mL^{-1} ampicillin sodium salt and 3% alginate solution. For comparison, alginate fiber without ampicillin was prepared as the control group. To observe the concentration effect of ampicillin, we fabricated IPA-24 h-fiber with different sample solutions containing 2, 1, 0.5, 0.1, 0.01, and 0 mg mL^{-1} ampicillin sodium salt in 3% alginate solutions. For the bacterial test, we prepared the agar plates coated with a mixture of dilute agar and *S. aureus*, placed the prepared drug loaded fibers of the same amount, and cultured these plates overnight in the incubator at 37 °C, allowing for formation of the bacteria lawns. After 24 h, the antibiotic activity of the drug released from the fiber was

measured by comparing the zones of inhibition per each sample fiber.

Fabrication of antibiotic fiber loaded wound dressing scaffolds

Chitosan powder (600 mg) was dispersed in 30 mL of 1% w/w of acetic acid, stirred overnight, and filtered. Prepared fibers (DW-24 h-fiber and IPA-24 h-fiber each) were distributed into PDMS cylindrical mold of 8 mm diameter, and then 80 μL chitosan solution was poured into the mold. They were immediately frozen in a −80 °C freezer for 6 hours, and then freeze-dried for at least 24 hours to form a porous sponge structure. The drug-loaded alginate fiber/chitosan scaffolds were sterilized using an EO gas system.

In vivo studies and evaluation procedures

Sprague–Dawley rats weighing 200–250 g were used for *in vivo* full thickness skin wound healing experiments. All animal experiments were approved by the Animal Care and Use committee of Korea University (KUIACUC-2014-80). Animals were anaesthetized with zoletil (6 mg kg^{-1}) and rompun (4 mg kg^{-1}), and then shaved on the back. The operative area of skin was cleaned with alcohol and an 8 mm punch biopsy was performed to construct a full-thickness excisional wound. For studies involving *S. aureus* wound infection, 80 μL of the bacterial suspension (10^{10} cells per mL) was applied to the surface of the wound, excepting the control group site. Two types of prepared wound dressing scaffolds (DW-24 h-fiber scaffold, IPA-24 h-fiber scaffold) were used to cover the wounds of each rat, and several sites were left without any treatment to only observe the bacterial effect. The operative sites were covered by dressing band (Medi-korea, Seoul, Korea) for protection and all rats were sacrificed 3 days after surgery. A sample from the wound area was harvested and fixed in a 4% PFA solution for histology. Fixed tissue specimens were embedded in paraffin wax, sectioned to 4 μm, and then stained with hematoxylin and eosin (H and E) for image analysis.

Statistics

Data are expressed as mean ± standard deviation (SD). Statistically significant differences were calculated with student's *t*-test or ANOVA one-way test (Sigma plot, Systat, Software Inc., San Jose, CA, USA). Differences were considered significant at $P < 0.05$.

Results and discussion

Loading of drug

The total amount of loaded ampicillin in the equal mass of four fiber groups (DW-0 h-fiber, DW-24 h-fiber, IPA-0 h-fiber, and IPA-24 h-fiber) was measured, and the results are summarized in Table 1. Total amount of loaded ampicillin was 57.6 ± 9.0 μg in the DW-0 h-fiber, and 10.8 ± 5.6 μg in the DW-24 h-fiber. In contrast, the IPA-based fibers entrapped larger amounts of drugs, 282.4 ± 4.2 μg in the IPA-0 h-fiber, and 356.5 ± 11.1 μg in the IPA-24 h-fiber. The DW-based fabrication method did not entrap a large quantity of ampicillin molecules within the fiber scaffolds compared to the IPA-based fabrication method. During the DW-based fabrication and washing processes, the ampicillin might be diffused into the surrounding solution, and only a small amount remained within the fiber. In the case of the DW-24 h-fiber, almost all of the ampicillin had been depleted, possibly because most of the loaded ampicillin was released due to the swelling during the curing process in DW solution. By contrast, the amounts of ampicillin initially loaded in the IPA-fiber were much higher than in the water-based fiber.

Table 1 Average ampicillin loaded into the fiber scaffolds. Different concentrations of the drugs were entrapped in the fibers for each process. The mean and standard deviations are reported ($N = 3$)

	DW-0 h-fiber	DW-24 h-fiber	IPA-0 h-fiber	IPA-24 h-fiber
Average loaded ampicillin in a 10 mg fiber [μg]	57.6 ± 9.0	10.8 ± 5.6	282.4 ± 4.1	356.5 ± 11.1

The drug loading in the alginate fiber matrix was visualized by replacing the ampicillin sodium salt with the fluorescent nanoparticles in each fiber fabrication process. Fig. 2a and b show confocal images of the fluorescent nanoparticle-loaded DW-24 h-fiber and IPA-24 h-fiber. Although the same concentration of particles was dissolved in the core solution, the fluorescence intensity was highest in the IPA-24 h-fiber, with a dense particle distribution; in contrast, the DW-24 h-fiber displayed low fluorescence intensity with a sparse distribution of particles in the swollen morphology. (Fig. 2c) This indicates that the condensed fiber structures created by the IPA-based fabrication process have superior drug loading capabilities compared to those created by the DW-based fabrication process (Fig. 2d and e).

In our previous report, we introduced a novel spinning method to create crystal-like ordered fibers as a result of the molecular repulsion by polarity, dehydration of the aqueous phase, and shear stress.[24] During the spinning process, IPA might promote the self-aggregation among the alginate polymer chains through dipole–dipole interactions between the core and sheath flows. This study shows that the alginate polymers acquire a highly ordered structure while simultaneously incorporating the ampicillin molecules in the polymer matrix as large as possible when the IPA is used as the sheath. However, when using the DW sheath, the alginate polymer solidified with a looser, non-crystalline structure. Thus, during the fiber fabrication process, ampicillin easily diffused out of the hydrated alginate polymer, due to its high solubility in water. Taken together, the drug entrapment ability of alginate was significantly enhanced by the dense crosslinking and dehydration process with the IPA sheath fiber spinning method in comparison with DW sheath flow.

Morphological changes

Fig. 3 shows four groups of fibers (DW-0 h-fiber, DW-24 h-fiber, IPA-0 h-fiber, and IPA-24 h-fiber) on day 0 (dried original fiber),

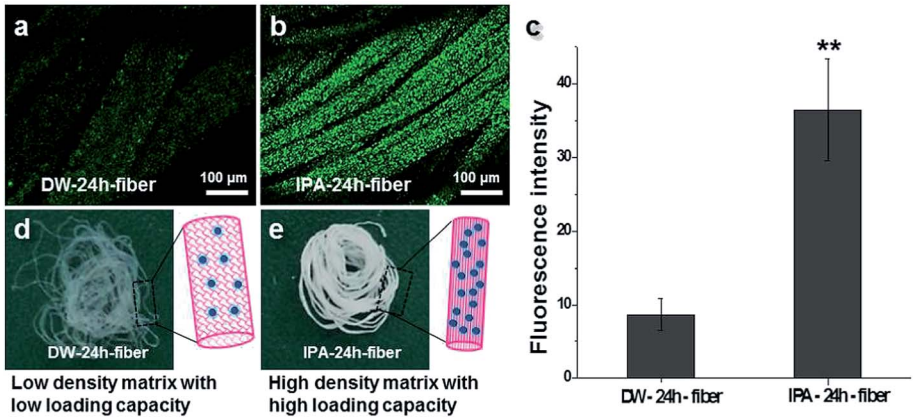

Fig. 2 (a) Confocal image of a fluorescent nanoparticle-loaded DW-24 h-fiber. (b) Confocal image of a fluorescent nanoparticle-loaded IPA-24 h-fiber. (c) Quantification of the fluorescence intensity using Image J. Bars indicate means ± SD. $^{**}P < 0.01$. (d) Dried DW-24 h-fiber scaffold and illustration of a drug-loaded fiber structure. (e) Dried IPA-24 h-fiber scaffold and illustration of a drug-loaded fiber structure.

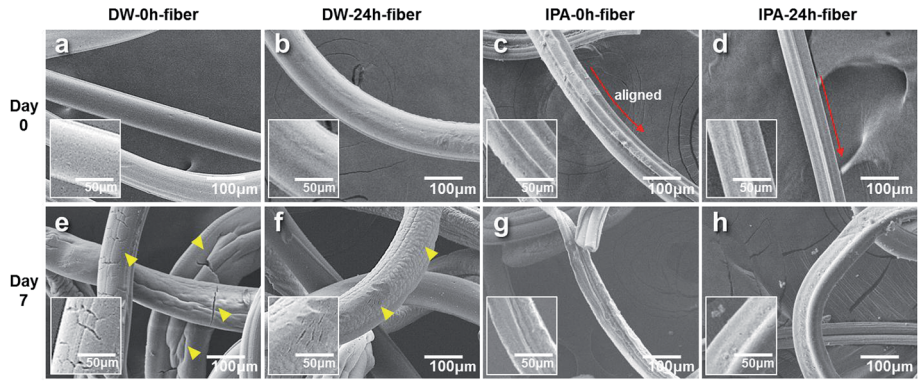

Fig. 3 SEM images of alginate fibers containing ampicillin at days 0 and 7 after immersion in PBS. (a) Fibers fabricated using the DW sheath flow, followed by immediate washing (DW-0 h-fiber). (b) Fibers fabricated using the DW sheath flow, followed by further coagulation in a 10% $CaCl_2$-DW coagulation bath for 24 h (DW-24 h-fiber). (c) Fibers fabricated using the IPA sheath flow, followed by immediate washing (IPA-0 h-fiber). (d) Fibers fabricated using the IPA sheath flow, followed by further coagulation in a 10% $CaCl_2$-IPA coagulation bath for 24 h (IPA-24 h-fiber). (e) DW-0 h-fiber after immersion in PBS for 7 days. (f) DW-24 h-fiber after immersion in PBS for 7 days. (g) IPA-0 h-fiber after immersion in PBS for 7 days. (h) IPA-24 h-fiber after immersion in PBS for 7 days.

and 7 days after immersion in PBS. At day 0, the DW-based fibers (DW-0 h-fiber and DW-24 h-fiber) displayed smooth round shapes without any cracks (Fig. 3a and b); however, on day 7, fractures, wrinkles, and irregular pores in surfaces became apparent, indicating that the fiber structure networks underwent a deformation transition (Fig. 3e and f). By contrast, the IPA-based fibers (IPA-0 h-fiber and IPA-24 h-fiber) displayed distinct morphological features. At day 0, the fibers had condensed, and their morphologies had aligned structures, yielding a smaller diameter compared to the DW-based fibers (Fig. 3c and d). These morphologies persisted in the PBS solution until day 7, without displaying any noticeable surface changes or degradation (Fig. 3g and h). No significant morphological differences were observed between the IPA-0 h-fiber and IPA-24 h-fiber.

Overall, the data indicated that the IPA based fabricated fibers showed less swelling and degradation profile during immersion in PBS. These results suggested that the conformational changes by IPA enhanced the polymer network with the compact structure and prolonged the degradation time scale.

Mass loss

The rate and extension of drug release depended on the erosion of the hydrated polymer; therefore, we quantitatively investigated the degree of fiber degradation upon incubation at 37 °C in the PBS solution. Fig. 4 shows the weight loss curves obtained from each group of fibers. These results revealed that the water-based groups degraded faster than the IPA-based groups, and the calcium coagulation time affected the degradation. The DW-0 h-fiber was almost fully dissolved after 7 days' incubation period in the PBS solution, presenting the fastest degradation timescale with a mass loss of 94.4 ± 3.5%. In contrast, the IPA-24 h-fiber showed the slowest degradation timescale, with a mass loss of 34.9 ± 2.0% at day 7. The second slowest

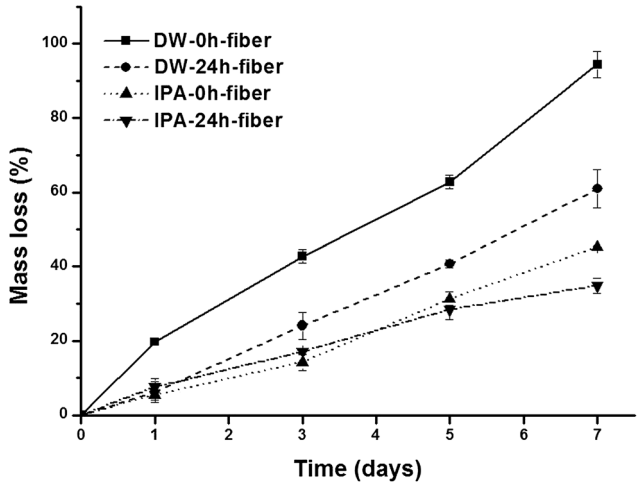

Fig. 4 Degradation profiles of the alginate fibers. Mass loss (%) = $[(W_i - W_f)/W_i] \times 100$, where W_i denotes the initial weight of the fiber and W_f indicates the weight of the partially eroded samples. The mean and standard deviation are reported ($N = 3$).

degradation group was the IPA-0 h-fiber, with a mass loss of 45.3 ± 0.2%, and the third slowest degradation group was the DW-24 h-fiber, with a mass loss of 60.9 ± 5.1%. Overall, these results indicated that the IPA sheath fibers formed a stronger alginate polymer crosslink resulting in a delayed mass loss. The 24-calcium-treated group displayed less mass erosion compared to the untreated group. These trends agreed with the morphological studies conducted previously (Fig. 3).

Release of drug

The release profiles of the four groups of antibiotic fibers (DW-0 h-fiber, DW-24 h-fiber, IPA-0 h-fiber, and IPA-24 h-fiber) were examined by dipping the fibers in PBS up to 7 days. The release behavior is plotted in Fig. 5. The release profile revealed a burst of ampicillin emission within the first 24 hours from the DW-based group. In particular, the profile showed that more than 80% of the initially loaded drug had been diffused out of the DW-24 h-fiber. The release of ampicillin from the IPA-24 h-fiber displayed a profile that fluctuated periodically until the solution concentration reached a constant value.

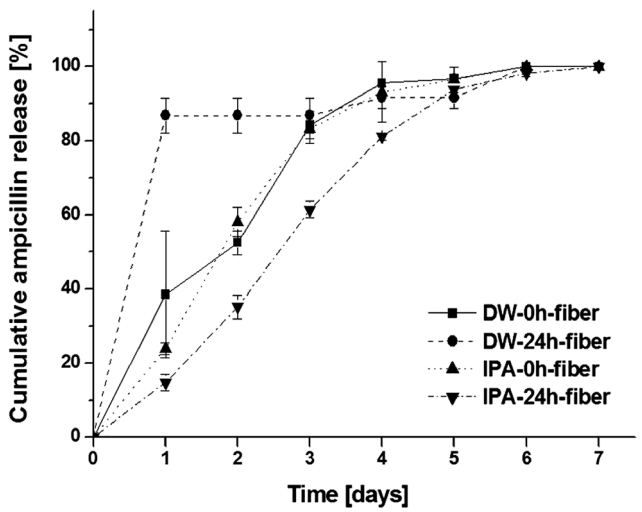

Fig. 5 *In vitro* testing of the ampicillin-releasing fibers. Cumulative release profiles of the ampicillin from the alginate fibers immersed in PBS. The mean and standard deviation are reported ($N = 3$).

Overall, the drug release from the IPA-fibers was delayed more than that from the DW-fibers, and the release profile was slightly slower in the calcium coagulation group. Although the DW-24 h-fiber exhibited faster release than the DW-0 h-fiber within 24 hours, the reason might be that during 24 hours curing in the DW solution and following the washing step, ampicillin seems to be already on the releasing phase due to the swelling and damaging of the alginate fiber.

The differences in the drug loading capacities (Table 1) and the release profiles for the DW- and IPA-based processes were thought to arise from the condensed aggregation of the polymer with the drug molecules. The degree of hydration and swelling of alginate polymers depended on the degree of crosslinking and influenced the drug release profile.[32–34] The drug molecules appeared to have been entrapped within the highly ordered alginate polymer network with a higher loading density, indicating that the densely aggregated structures also influenced the release profiles. In summation, the IPA-24 h-fiber proved more befitting as a drug-carrier than others because of its delayed release of loaded drugs.

ATR-FTIR and XRD analysis for structural characterization

FTIR and XRD analysis were conducted to evaluate the fiber crystallinity. For FTIR analysis, pure alginate, DW-24 h-fiber and IPA-24 h-fiber were examined (Fig. 6a). Pure alginate displays a characteristic functional band (–COO group) with a broad asymmetrical band at 1600 cm^{-1} and a narrower symmetrical band at 1417 cm^{-1}. A wide absorption band appears around 3300 cm^{-1} due to vibrations of the hydroxyl groups (OH). The spectra of the drug-loaded fibers displayed a similar absorption band to that of alginate. The IPA-24 h-fiber showed strong sharp peaks; however, additional peaks or noticeable shifts were not observed. Fig. 6b shows one-dimensional X-ray diffraction patterns of the fibers from IPA-based (black line) and DW-based (red line) sheath fluids, respectively. Both patterns were similar, as the peaks in both groups were observed at $2\theta = 23.80°$ in the spectra. The strengths of the 2θ patterns in the spectra reflected the degree of crystallinity. IPA-based alginate fibers provide little sharper and stronger diffraction peaks, which indicate higher crystallinity and a more perfect ordering, compared to the fibers fabricated with the water-based sheath flow. Therefore, these results suggest that the solvent system induces conformational changes to a condensed ordered structure by dehydration. This could explain why the IPA sheath based fibers exhibited a more enhanced drug loading capability than the DW sheath fibers did.

Antibiotic activity

The antibiotic activity of the DW-based and IPA-based ampicillin-loaded fiber was measured by exposing the fiber

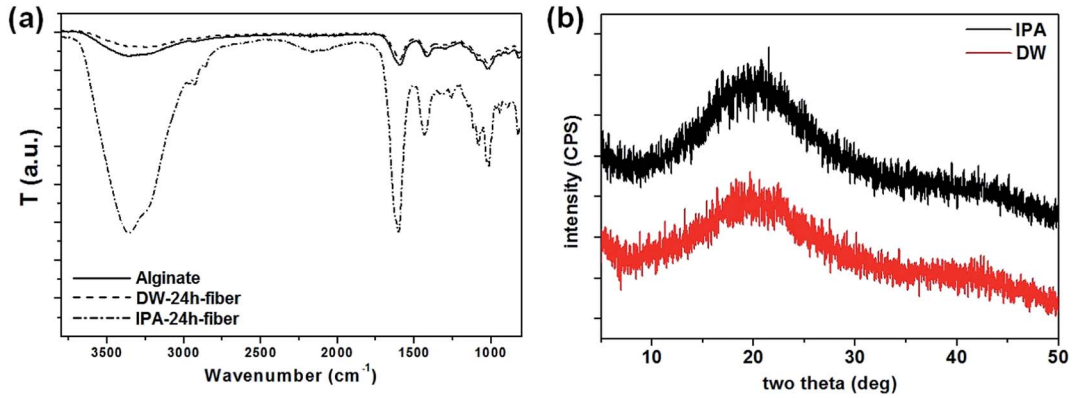

Fig. 6 (a) The FT-IR spectra of the alginate fibers (black line), DW sheath ampicillin-loaded fibers (dashed line) and IPA sheath ampicillin-loaded fibers (dash dot line). (b) The XRD patterns of the alginate fibers prepared by using an IPA-based sheath solution (black line) or a DW-based sheath solution (red line).

scaffolds to cultures of *S. aureus*. The bacterial growth was observed directly from the plate to assess the efficacy of the drug-loaded fibers. The clear area around the fiber scaffold without any bacterial growth (Fig. 7) was defined as the zone of inhibition. Only IPA-24 h-fibers showed inhibition of the bacterial growth through the diffusion of the drug onto the agar (Fig. 7a and b). In contrast, DW-24 h-fibers had no inhibitory effect, similar to pure alginate fibers. Although the same concentration of antibiotic (1 mg mL^{-1}) was used in both the IPA and DW based fiber fabrication process, the IPA based fabrication method enabled more entrapping of drug molecules in the fiber matrix than the DW based method, as discussed

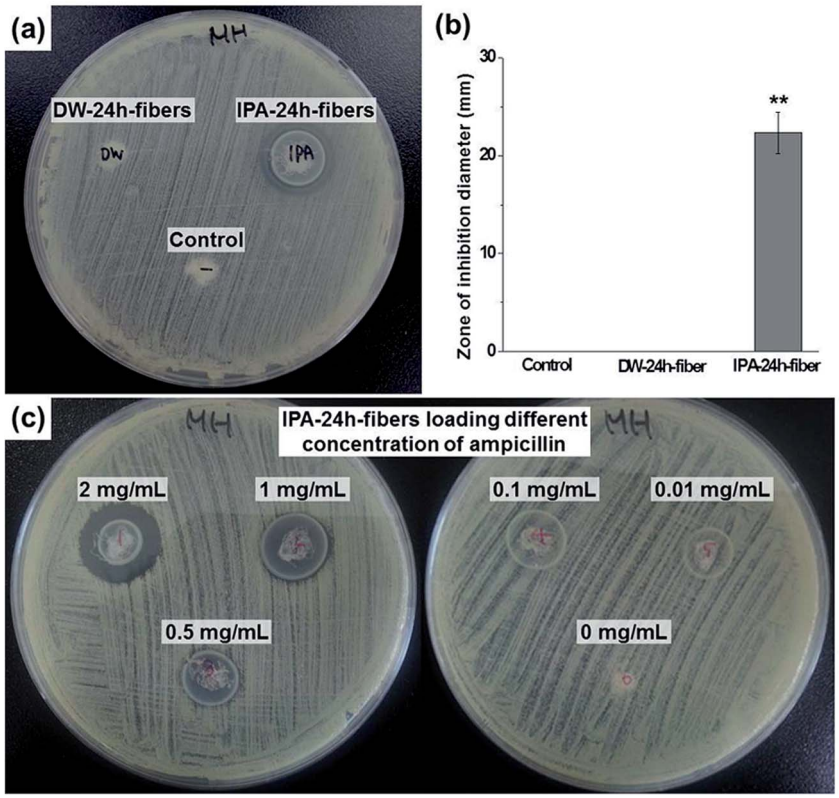

Fig. 7 Antibacterial activity induced by the fiber scaffolds against *S. aureus*. (a) Representative sample agar plates showing the zone of inhibition formed by DW-24 h-fibers, IPA-24 h-fibers and control fiber scaffolds (5 mg of each fiber sample was applied). (b) Each bar represents the mean diameter of the zone of inhibition resulting in three independent scaffolds ($N = 5$). $^{**}P < 0.01$. (c) The IPA-24 h-fibers were fabricated with different concentrations of the ampicillin/alginate solution 2 mg mL^{-1}, 1 mg mL^{-1}, 0.5 mg mL^{-1}, 0.1 mg mL^{-1}, 0.01 mg mL^{-1} and 0 mg mL^{-1} (control). (5 mg of each fiber sample was applied.)

previously. Furthermore, to decide on a suitable ampicillin loading condition *in vivo*, we loaded different concentrations of ampicillin—ranging from 0.1 mg mL^{-1} to 2 mg mL^{-1}—into the alginate fibers fabricated with the IPA sheath. The alginate fiber with 2 mg mL^{-1} of ampicillin showed the best inhibitory effect compared to other groups, as shown in Fig. 7c. In addition, these results indicated that the loading concentration of ampicillin in the fibers could be regulated by changing the initial concentration of drug in the polymer solution. Taken together, the antibiotic loaded fiber fabricated using the IPA sheath flow was proven superior to those fabricated using DW sheath flow, with a higher antibiotics biological efficacy.

Effect of antibiotic fiber incorporated into chitosan scaffold on infected wound

The wound healing process involves overlapping phases of inflammation, cell migration and proliferation, neovascularization, extracellular matrix production, and remodelling.[35] However, in this study, we observed only the early phase of the process to assess the therapeutic efficacy of antibiotic fiber scaffolds at the initial stage of infection *in vivo*. We utilized a SD rat model of *S. aureus* bacterial infected wound, and applied the fabricated scaffold (Fig. 8a–c). Total of four groups were observed: (1) uninfected wound, (2) the bacterial infected wound without treatment, the bacterial infected wound treated with either (3) DW-24 h-fiber scaffold or (4) IPA-24 h-fiber scaffold. A consistent concentration of bacterial solution was applied to each wound-site for infection. Early stage wound size reduction was improved in the case of bacterial infected wound treated with IPA-24 h-fiber scaffold, compared to all other cases (Fig. 8d). Groups (2) and (3) showed no area difference in the early stages of healing. However, significant distinctions were observed between the groups on the histological analysis. (Fig. 8e–h) At 3 days of post-wounding, inflammation was observed in every group with lymphocytes and monocytes. Necrosis area was observed in groups (2), (3), and (4), indicating that the bacterial wound infection established successfully. This phenomenon was most severe in group (2). Scaffold (DW-24 h-fiber and IPA-24 h-fiber) treated groups (group (3) and (4)) showed a positive effect compared to group (2). It is likely that the presence of the scaffold affected the wound healing with an antimicrobial effect of chitosan.[36] However, it was clear that the antibacterial ability of the IPA-24 h-fiber scaffold was superior to DW-24 h-fiber as it shows less necrosis area and a similar state to the uninfected control group (group (1)). The IPA-24 h-fiber scaffold had better antibacterial effects on the wound, which suggests that it had more antibiotic drug loaded during the fabrication process. In this work, the IPA-24 h-fiber scaffold shows the strongest antibacterial properties for

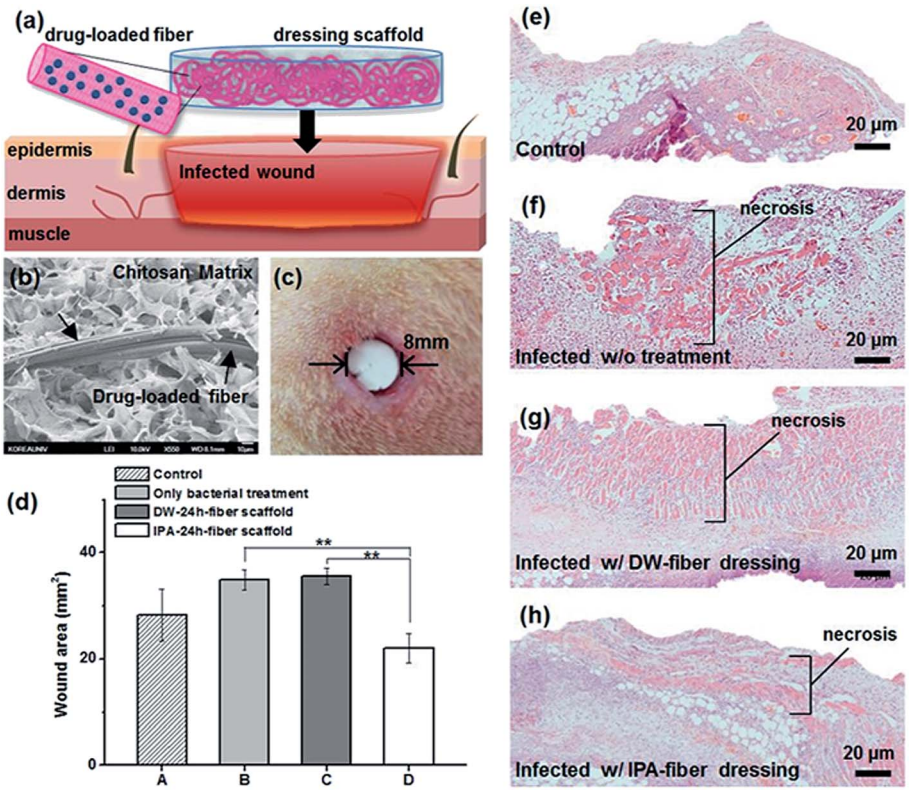

Fig. 8 (a) A schematic diagram illustrating the full thickness bacterial infected wounds with dressing scaffold incorporating drug loaded fibers. (b) SEM image of cross-sectional dressing scaffold. Black arrows indicate alginate drug-loaded fiber in the porous chitosan matrix. (c) Macroscopic observation of excisional wound immediately after wounding. (d) Remaining wound area after 3 days of repair. Bars indicate mean ± SD. $^{**}P < 0.01$. Histological examination of wounds on day 3 (e) Control group (no bacterial treatment, no scaffold), (f) bacteria infected without treatment group, (g) bacteria infected and DW-24 h-fiber wounding group, (h) bacteria infected and IPA-24 h-fiber wounding group.

wound-dressing with a desirable biocompatibility and physical characteristics of the alginate and chitosan complex. Although we focused only on the antibiotic drug delivery wound dressing scaffold, this can be applied on various areas with enhanced drug loading and stable delivery performance.

Conclusions

We developed a simple micro-fluidic spinning method for fabrication of antibiotic-loaded alginate fibers with enhanced drug-loading capability. The IPA sheath flow was shown to promote the confinement of ampicillin molecules within the fiber because the dehydration process lead to condensed ordering of the alginate polymer. These IPA sheath based fiber also showed more delayed degradation and release profile than the DW sheath fibers without damaging the antibiotic effects both *in vitro* and *in vivo*. Several reports have indicated that alginate is suitable for use in the extended release of a range of antibiotics (penicillin, ampicillin, gentamicin, and vancomycin).[37–40] As alginate has also notably been used as a wound dressing material,[31,41–44] we demonstrated our antibiotic-loaded fiber scaffold for the wound healing of rat's skin, and we observed that delivered drug played a positive role to the infected wound. The proposed microfluidic spinning method will extend its applications even to the drug delivery fields, and could create diverse clinically applicable products for wound healing.

Acknowledgements

This work was supported by the National Research Foundation of Korea (NRF), funded by the Korean Government (MEST) (no. 2013046403).

References

1 V. Sinha and A. Trehan, Biodegradable microspheres for protein delivery, *J. Controlled Release*, 2003, **90**, 261–280.
2 K. S. Soppimath, T. M. Aminabhavi, A. R. Kulkarni and W. E. Rudzinski, Biodegradable polymeric nanoparticles as drug delivery devices, *J. Controlled Release*, 2001, **70**, 1–20.
3 E. Soussan, S. Cassel, M. Blanzat and I. Rico-Lattes, Drug delivery by soft matter: matrix and vesicular carriers, *Angew. Chem., Int. Ed.*, 2009, **48**, 274–288.
4 S. Svenson and D. A. Tomalia, Dendrimers in biomedical applications—reflections on the field, *Adv. Drug Delivery Rev.*, 2012, **64**, 102–115.
5 M. Schäfer-Korting, W. Mehnert and H.-C. Korting, Lipid nanoparticles for improved topical application of drugs for skin diseases, *Adv. Drug Delivery Rev.*, 2007, **59**, 427–443.
6 N. Bhattarai, J. Gunn and M. Zhang, Chitosan-based hydrogels for controlled, localized drug delivery, *Adv. Drug Delivery Rev.*, 2010, **62**, 83–99.
7 Q. Wang, X. Hu, Y. Du and J. F. Kennedy, Alginate/starch blend fibers and their properties for drug controlled release, *Carbohydr. Polym.*, 2010, **82**, 842–847.
8 H. H. Tønnesen and J. Karlsen, Alginate in drug delivery systems, *Drug Dev. Ind. Pharm.*, 2002, **28**, 621–630.
9 O. Smidsrød, R. M. Glover and S. G. Whittington, The releative extension of alginates having different chemical composition, *Carbohydrate research*, 1973, **27**(1), 107–118.
10 O. Smidsrød and G. Skjåk-Braek, Algiante as immobilization matrix for cells, *Trends Biotechnol*, 1990, **8**, 71–78.
11 Y. M. Elcin, V. Dixit and G. Gitnick, Extensive in vivo angiogenesis following controlled release of human vascular endothelial cell growth factor: implications for tissue engineering and wound healing, *Artif. Organs*, 2001, **25**, 558–565.
12 H. Tanaka, M. Matsumura and I. A. Veliky, Diffusion characteristics of substrates in Ca-alginate gel beads, *Biotechnol. Bioeng.*, 1984, **26**, 53–58.
13 D. H. Kim and D. C. Martin, Sustained release of dexamethasone from hydrophilic matrices using PLGA nanoparticles for neural drug delivery, *Biomaterials*, 2006, **27**, 3031–3037.
14 C. Y. Yu, X. C. Zhang, F. Z. Zhou, X. Z. Zhang, S. X. Cheng and R. X. Zhuo, Sustained release of antineoplastic drugs from chitosan-reinforced alginate microparticle drug delivery systems, *Int. J. Pharm.*, 2008, **357**, 15–21.
15 K. Moebus, J. Siepmann and R. Bodmeier, Alginate-poloxamer microparticles for controlled drug delivery to mucosal tissue, *Eur. J. Pharm. Biopharm.*, 2009, **72**, 42–53.
16 H. Tanaka, M. Matsumura and I. Veliky, Diffusion characteristics of substrates in Ca-alginate gel beads, *Biotechnol. Bioeng.*, 1984, **26**, 53–58.
17 S.-J. Shin, J.-Y. Park, J.-Y. Lee, H. Park, Y.-D. Park, K.-B. Lee, C.-M. Whang and S.-H. Lee, "On the fly" continuous generation of alginate fibers using a microfluidic device, *Langmuir*, 2007, **23**, 9104–9108.
18 C. M. Hwang, A. Khademhosseini, Y. Park, K. Sun and S.-H. Lee, Microfluidic chip-based fabrication of PLGA microfiber scaffolds for tissue engineering, *Langmuir*, 2008, **24**, 6845–6851.
19 Y. Jun, E. Kang, S. Chae and S.-H. Lee, Microfluidic spinning of micro-and nano-scale fibers for tissue engineering, *Lab on a Chip*, 2014, **14**, 2145–2160.
20 E. Kang, Y. Y. Choi, S. K. Chae, J. H. Moon, J. Y. Chang and S. H. Lee, Microfluidic spinning of flat alginate fibers with grooves for cell-aligning scaffolds, *Adv. Mater.*, 2012, **24**, 4271–4277.
21 E. Kang, G. S. Jeong, Y. Y. Choi, K. H. Lee, A. Khademhosseini and S.-H. Lee, Digitally tunable physicochemical coding of material composition and topography in continuous microfibres, *Nat. Mater.*, 2011, **10**, 877–883.
22 K. H. Lee, S. J. Shin, Y. Park and S. H. Lee, Synthesis of cell-laden alginate hollow fibers using microfluidic chips and microvascularized tissue-engineering applications, *Small*, 2009, **5**, 1264–1268.
23 K. HoáLee, S. JungáShin, J. KyungáKim, Y. WooáCho and B. GeunáChung, Microfluidic synthesis of pure chitosan microfibers for bio-artificial liver chip, *Lab Chip*, 2010, **10**, 1328–1334.

24 S. K. Chae, E. Kang, A. Khademhosseini and S. H. Lee, Micro/Nanometer-scale fiber with highly ordered structures by mimicking the spinning process of silkworm, *Adv. Mater.*, 2013, **25**, 3071–3078.

25 B. Barai, R. Singhal and P. Kulkarni, Optimization of a process for preparing carboxylmethyl cellulose from water hyacinth (Eichornia crassipes), *Carbohydr. Polym.*, 1997, **32**, 229–231.

26 C. K. Kuo and P. X. Ma, Ionically crosslinked alginate hydrogels as scaffolds for tissue engineering: part 1. Structure, gelation rate and mechanical properties, *Biomaterials*, 2001, **22**, 511–521.

27 G. Pasparakis and N. Bouropoulos, Swelling studies and in vitro release of verapamil from calcium alginate and calcium alginate-chitosan beads, *Int. J. Pharm.*, 2006, **323**, 34–42.

28 M. Davidovich-Pinhas and H. Bianco-Peled, A quantitative analysis of alginate swelling, *Carbohydr. Polym.*, 2010, **79**, 1020–1027.

29 P. Aslani and R. A. Kennedy, Studies on diffusion in alginate gels. I. Effect of cross-linking with calcium or zinc ions on diffusion of acetaminophen, *J. Controlled Release*, 1996, **42**, 75–82.

30 K. HoáLee, Novel PDMS cylindrical channels that generate coaxial flow, and application to fabrication of microfibers and particles, *Lab Chip*, 2010, **10**, 1856–1861.

31 R. Thakur, C. Florek, J. Kohn and B. Michniak, Electrospun nanofibrous polymeric scaffold with targeted drug release profiles for potential application as wound dressing, *Int. J. Pharm.*, 2008, **364**, 87–93.

32 E. Zactiti and T. Kieckbusch, Potassium sorbate permeability in biodegradable alginate films: Effect of the antimicrobial agent concentration and crosslinking degree, *J. Food Eng.*, 2006, **77**, 462–467.

33 X. Shu and K. Zhu, The release behavior of brilliant blue from calcium–alginate gel beads coated by chitosan: the preparation method effect, *Eur. J. Pharm. Biopharm.*, 2002, **53**, 193–201.

34 K. Wang and Z. He, Alginate–konjac glucomannan–chitosan beads as controlled release matrix, *Int. J. Pharm.*, 2002, **244**, 117–126.

35 S. Froget, E. Barthelemy, F. Guillot, C. Soler, M. C. Coudert, M. Benbunan and C. Dosquet, Wound healing mediator production by human dermal fibroblasts grown within a collagen-GAG matrix for skin repair in humans, *Eur. Cytokine Network*, 2003, **14**, 60–64.

36 E. I. Rabea, M. E. T. Badawy, C. V. Stevens, G. Smagghe and W. Steurbaut, Chitosan as antimicrobial agent: applications and mode of action, *Biomacromolecules*, 2003, **4**, 1457–1465.

37 G. C. Fontes, V. M. Calado, A. M. Rossi and M. H. da Rocha-Leao, 2013 Characterization of antibiotic-loaded alginate-OSA starch microbeads produced by ionotropic pregelation, *BioMed Res. Int.*, 2013, 472626.

38 S. W. Ueng, L. J. Yuan, N. Lee, S. S. Lin, E. C. Chan and J. H. Weng, In vivo study of biodegradable alginate antibiotic beads in rabbits, *J. Orthop. Res.*, 2004, **22**, 592–599.

39 M. Bohner, J. Lemaître, P. V. Landuyt, P. Y. Zambelli, H. P. Merkle and B. Gander, Gentamicin-loaded hydraulic calcium phosphate bone cement as antibiotic delivery system, *J. Pharmaceut. Sci.*, 1997, **86**, 565–572.

40 T. Hou, J. Xu, Q. Li, J. Feng and L. Zen, In vitro evaluation of a fibrin gel antibiotic delivery system containing mesenchymal stem cells and vancomycin alginate beads for treating bone infections and facilitating bone formation, *Tissue Eng., Part A*, 2008, **14**, 1173–1182.

41 T. Hashimoto, Y. Suzuki, M. Tanihara, Y. Kakimaru and K. Suzuki, Development of alginate wound dressings linked with hybrid peptides derived from laminin and elastin, *Biomaterials*, 2004, **25**, 1407–1414.

42 C. J. Knill, J. F. Kennedy, J. Mistry, M. Miraftab, G. Smart, M. R. Groocock and H. J. Williams, Alginate fibres modified with unhydrolysed and hydrolysed chitosans for wound dressings, *Carbohydr. Polym.*, 2004, **55**, 65–76.

43 L. Wang, E. Khor, A. Wee and L. Y. Lim, Chitosan-alginate PEC membrane as a wound dressing: Assessment of incisional wound healing, *J. Biomed. Mater. Res.*, 2002, **63**, 610–618.

44 S. Huang and X. Fu, Naturally derived materials-based cell and drug delivery systems in skin regeneration, *J. Controlled Release*, 2010, **142**, 149–159.